COMPARISON OF ANALYTICAL AND FINITE ELEMENT BASED LIMIT LOADS FOR WIDE PLATES CONTAINING AN EXTENDED SURFACE CRACK UNDER COMBINED BIAXIAL FORCES AND CROSS-THICKNESS BENDING

Chris Aird[1], Yuebao Lei[1]

[1] Structural Integrity Engineer, Assessment Technology Group, EDF Energy, UK

ABSTRACT

This paper compares von Mises based analytical limit loads for a wide plate containing an extended surface crack under combined biaxial forces and cross-thickness bending with limit loads derived using finite element analysis. Differences between the analytical and finite element based limit load solutions are shown to exist as a result of compatibility being enforced in the finite element calculations. These differences are found to be relatively small when the net moment acting on the ligament is reduced to zero. For other loading conditions it is shown that the analytical limit loads can be significantly lower than the associated finite element values. Use of the analytical limit loads in these cases may result in an overly conservative estimate of the proximity of the structure to plastic collapse.

INTRODUCTION

In the late 1970s, Lee and Liebowitz (1977) carried out work on the influence of biaxial loading on the J integral fracture parameter. In the twenty or so years following this, a large body of work relating to the effect of biaxial loading on fracture was produced. A number of researchers, including Jansson (1986) and O'Dowd et al. (1999), addressed the influence of biaxial loading on the J integral and related crack-tip parameters. Others, including Jones et al. (1986), Bass et al. (1994) and Margolin and Kostylev (1998) considered the effect of biaxial loading on the apparent fracture toughness of a range of engineering materials. Much of the relevant numerical and analytical work carried out during this period focused on centre-cracked plates under biaxial forces.

More recently, Kim et al. (2004), Wang (2006) and Miura and Takahashi (2007) have derived J integrals and constraint parameters for surface cracked plates under the action of biaxial forces. Miura and Takahashi (2009) subsequently extended their work to include the influence of cross-thickness bending in addition to biaxial forces. Work in a similar vein was carried out by Wei and Hadley (2012) who considered the influence of biaxial loading on the integrity of surface cracked plates and pipes. Following this, Meek and Ainsworth (2014a, 2014b) revisited the centre-cracked plate under biaxial loading and carried out limit load and J integral calculations which cover a wider range of biaxiality ratios than previous work.

In assessing the integrity of both cracked and uncracked structures, the factor by which the applied primary loads, P, would have to be increased in order to cause plastic collapse is an important consideration. For example, within the UK R6 procedure (2015) for assessing the integrity of structures containing defects the proximity of a loaded structure to plastic collapse is determined by calculating an associated elastic perfectly-plastic "limit load" P_L and hence the value of the parameter $L_r = P/P_L$. Plastic collapse is avoided if L_r is less than a limiting value, L_r^{max}. Within R6 the L_r parameter also dictates the assumed ratio between the elastically calculated J integral and the corresponding elastic-plastic value. Limit load solutions are commonly calculated on an analytical basis using the lower bound theorem of plasticity together with an appropriate yield condition.

In order to enable the structural integrity of surface cracked plates under the action of combined biaxial forces and cross-thickness bending to be assessed within the R6 procedure (2015) appropriate limit load solutions have recently been developed by Lei (2014a) and Lei and Budden (2014c). These analytical solutions are based on the lower bound theorem of plastic collapse. The present paper builds on preliminary work by Lei et al. (2014b) and restricts attention to a comparison of Lei's analytical limit loads with those derived using finite element analysis. Estimation of J based on these limit loads is left to future publications. The particular case of a plate containing an extended surface crack under combined biaxial forces and cross-thickness bending is considered.

ANALYTICAL LIMIT LOAD SOLUTIONS

Figure 1 shows the cracked plate together with a force *N* acting in the direction perpendicular to the crack plane at the centroid of the section at the ends of the plate, a stress σ_x acting parallel to the crack front and a cross-thickness bending moment *M*. The positive directions of *N*, σ_x and *M* are shown. Positive *N* corresponds to tensile end force. Positive σ_x corresponds to tensile stress parallel to the crack plane. Positive *M* corresponds to a cross-thickness bending moment which acts to open the crack mouth.

Lei's limit load solutions (2014b), (2014c) are based on an elastic perfectly-plastic material and assume the only stresses acting on the ligament to be direct stresses in the *z* (crack opening) direction and, in the case of an applied stress σ_x, in the *x* direction (parallel to the crack front). Crack face contact is ignored. The crack length *a* is expressed in non-dimensional form as

$$\alpha = a/t \tag{1}$$

Non-dimensional limit loads for *N*, *M* and σ_x, respectively, at the point of collapse are defined as

$$n_L = N_L/(2Wt\sigma_y) \tag{2}$$

$$m_L = 2M_L/(Wt^2\sigma_y) \tag{3}$$

$$n_{xL} = \sigma_{xL}/\sigma_y \tag{4}$$

where σ_y is the uniaxial yield strength. Proportional loading is assumed and the following non-dimensional load ratio, relating the applied bending moment *M* to the end force *N,* is defined

$$\lambda = M/(tN) = m_L/(4n_L) \tag{5}$$

A similar non-dimensional load ratio relating the out-of-plane stress σ_x to the end force *N* is also defined

$$\lambda_1 = \sigma_x/(N/(2Wt)) = n_{xL}/n_L \tag{6}$$

In the case with the ends of the plate being unrestrained, but ignoring large displacement effects, use of a von Mises yield criterion enables the normalised limit load n_L to be calculated for any normalised crack length α and any given combination of *N*, *M* and σ_x, as defined by the non-dimensional parameters λ and λ_1. Providing a solution which covers each of the four quadrants of n_L - m_L space requires the particular value of the load ratio λ corresponding to zero net moment acting on the ligament to be identified. Denoting this value as λ_0 it can be expressed as

$$\lambda_0 = -\alpha/2 \tag{7}$$

Then, for combinations of *N* and *M* which give a positive (crack opening) moment at the ligament the normalised limit load n_L is

$$n_L = \sqrt{\frac{1}{D^2+3(\lambda_1 E)^2}\left(2E^2+CD-\sqrt{(2E^2+CD)^2-(D^2+3(\lambda_1 E)^2)C^2}\right)} \tag{8}$$

for $(\lambda-\lambda_0)\geq 0$, $N\geq 0$ and

$$n_L = -\sqrt{\frac{1}{D^2+3(\lambda_1 E)^2}\left(2E^2+CD-\sqrt{(2E^2+CD)^2-(D^2+3(\lambda_1 E)^2)C^2}\right)} \tag{9}$$

for $(\lambda-\lambda_0)<0$, $N<0$ where $C=(1-\alpha)^2$, $D=1-(1-\alpha)\lambda_1+((1-\alpha)\lambda_1)^2$ and $E=2\lambda+\alpha$. The corresponding values of m_L can be calculated using Equation 5. The equivalent expressions for combinations of *N* and *M* which give a negative (crack closing) moment at the ligament are, respectively, an equation identical to Equation 9 for $(\lambda-\lambda_0)\geq 0$, $N\leq 0$ and an equation identical to Equation 8 for $(\lambda-\lambda_0)<0$, $N>0$.

FINITE ELEMENT MODELS

Figure 2 shows a 3D quarter-plate model typical of those used in the study. The associated boundary conditions, loading, material properties and element type are described below.

Boundary conditions:

- In addition to the displacement of the nodes lying on the symmetry planes being fixed in the perpendicular direction, the displacement of a single node at the top surface of the plate was fixed in the *y* direction. Rigid body motion was thereby prevented without over constraining the model.

Loading:

- The stress σ_x was applied as a surface pressure.
- The nodes at the free end of the plate were constrained to remain planar and the end force *N* and bending moment *M* were applied using a force couple – the first nodal force being applied to a node at the top surface of the plate, the second being applied to the corresponding node at the bottom surface.

Material properties:

- Each model used an elastic perfectly-plastic material law with a yield strength of 100 MPa, together with an assumed Young's modulus of 200 GPa and a Poisson's ratio of 0.3.

Element type:

- Reduced integration twenty-node quadratic elements were used.

Mesh refinement studies were carried out in order to ensure that a suitable mesh density was used. A small displacement approach was employed. Crack-face contact was not modelled. For tension dominated cases collapse was determined from the force versus displacement history at the end of the plate by identifying the point of intersection of a straight line, passing through the origin and with gradient one half that of the initial tangent to the force versus displacement curve, with the force versus displacement curve. For bending dominated cases collapse was determined from the moment versus rotation history in a similar manner. For intermediate cases, the limit load was taken the be the lower of the limit load derived from the force versus displacement curve and the corresponding limit load derived from the moment versus rotation curve. The calculations were carried out using Abaqus version 6.9 (2009).

COMPARISON OF ANALYTICAL AND FINITE ELEMENT BASED LIMIT LOADS

Given space limitations, for the purpose of this paper a single normalised crack length α of 0.25 is used. Three sets of results are presented. First, results from a study into the effect of plate width on the predicted collapse load under applied end force N are considered. Second, the collapse locus in n_L - m_L space predicted by a “wide plate” 3D model in the absence of out-of-plane stress σ_x is compared with the corresponding analytical locus. Third, the influence of out-of-plane stress on the predicted collapse loci is considered.

The Effect of Plate Width

Figure 3 presents normalised limit loads n_L corresponding to 3D models of varying width, each of which was subject to end force N only. Points (a) to (f) correspond to normalised plate half-widths W/t of 0.0208, 0.1875, 0.375, 0.75, 1.5 and 3 respectively. The analytical limit load is also plotted together with limit loads derived from 2D plane stress and plane strain FE models. Increasing the width of the 3D model can be seen to increase the predicted limit load from close to the level associated with the 2D plane stress model to close to the level associated with the 2D plane strain model. It was concluded that using a 3D model with a normalised plate half-width W/t of 1.5 or more was appropriate for a wide plate.

The differences between the analytical and the 2D plane stress and plane strain models are a result of the different stress states in the three cases. Both the analytical and plane stress cases are associated with zero out-of-plane stress. However, the analytical solution assumes that the only stresses acting on the ligament are direct stresses in the z (loading) direction, whereas, in the case of the 2D plane stress model, y (through-thickness) direction stresses are set up in the zone of contained yielding local to the crack tip and act to increase the limit load. The additional out-of-plane stresses which are set up in the plane strain model act to increase the limit load yet more.

Comparison of Failure Loci in n_L - m_L Space – Without Out-of-Plane Stress σ_x

Figure 4(a) compares the analytical failure locus in n_L - m_L space in the case with no out-of-plane stress with that of a wide plate 3D model (with W/t of 1.5). Results from a 2D plane strain model are also shown. The three failure loci are broadly similar in shape. Each locus has two tips which are associated with the maximum and minimum values of n_L respectively. In each case these tips lie on the straight line passing through the origin in n_L - m_L space which corresponds to the particular ratio of N to M which gives zero net moment at the ligament, that is $\lambda = \lambda_0$. Each locus is symmetric about this straight line.

There are also evident differences between the three failure loci. In general, the FE-based failure loci lie outside of the analytical locus with the difference between the FE-based and analytical loci varying with angular position θ in n_L - m_L space. This difference is shown in Figure 4(b) which plots ξ (the ratio of the radial position of each FE-based point in n_L - m_L space to that of the corresponding analytical value) as a function of θ. For the limited number of points considered, the 3D results show the ratio ξ to reach a minimum of 0.97 at the values of θ corresponding to the two tips of the failure loci and a maximum of 1.61 at θ of 45° and 225°. These minima and maxima correspond to the analytical solution giving an accurate estimate of the limit load in the former case but (conservatively) underestimating the limit load in the latter case by almost 40%. The 2D plane strain results show similar, but not identical, behaviour. The minimum and maximum values of ξ occur at the same values of θ as in the 3D case. However, it can be seen that the 2D plane strain ξ values are higher than the corresponding 3D values at all values of θ with the difference being largest at the tips of the failure locus. Again, the differences between the three limit loads solutions can be explained with reference to the underlying stresses. Additional stresses are generated in the FE models as a result of compatibility being enforced.

Comparison of Failure Loci in n_L - m_L Space – With Out-of-Plane Stress σ_x

Figure 5a plots analytical and 3D wide plate FE failure loci for cases with low ($|\lambda_1|=1/(1-\alpha)$) and high ($|\lambda_1|=5$) levels of compressive out-of-plane stress. For the purpose of comparison, the failure loci of Figure 4, which correspond to the case with no out-of-plane stress $|\lambda_1|=0$, are also shown. For those cases with $|\lambda_1|$ of $1/(1-\alpha)$ the magnitude of the out-of-plane compressive stress is identical to that of the ligament membrane stress associated with the end force *N*. In this case, the effect of the out-of-plane compression on the limit load is negligible when the applied end force is compressive but reduces the limit load significantly in those cases which are dominated by tensile end force. However, for those cases associated with $|\lambda_1|$ of 5 the compressive out-of-plane stress is significantly larger in magnitude than the ligament membrane stress associated with the applied end force, and a significant reduction in limit load can be seen both for cases of pure tensile end force and for cases of pure compressive end force. For pure bending, the limit load predictions for the different values of normalised out-of-plane stress are identical since, in each case, the end force and therefore the applied out-of-plane stress are both zero.

The differences between the FE and the analytical collapse loci are shown explicitly in Figure 5(b) which plots ξ values. The difference between the FE and analytical limit loads can be seen to vary with θ for each of the three values of $|\lambda_1|$ and to be minimised at or near to the tips of each collapse locus. Apart from for pure bending (θ = 90°, 180°), where the value of $|\lambda_1|$ has no effect on the limit load and therefore no effect on ξ, the effect of increasing the magnitude of $|\lambda_1|$ is to reduce the value of ξ.

CONCLUSIONS

The following conclusions were drawn from the work presented in this paper, which considered a free end plate with normalised crack depth α of 0.25:

1. A 3D finite element model with a normalised plate half-width *W/t* of at least 1.5 is required in order to give limit loads representative of a wide plate. (Note that Figure 1 shows the overall plate width to be *2W*, so that *W/t* of 1.5 corresponds to the overall width of the plate being three times the thickness.)
2. Limit loads calculated using a 2D plane strain model generally give a reasonably close approximation to the limit loads calculated from wide plate 3D FE models under combined cross-thickness bending and end force in the absence of out-of-plane stress.
3. Limit loads calculated from wide plate 3D FE models under combined cross-thickness bending and end force in the absence of out-of-plane stress generally exceed the corresponding analytical values, with the difference between the FE-based and analytical values being dependent upon the

ratio of the applied bending moment *M* to the end force *N*. The difference was seen to be minimised in those cases with zero net moment acting on the ligament.

4. The influence on limit load of applied out-of-plane stress σ_x predicted by the analytical limit load solution is consistent with that seen in the 3D wide plate FE models. As in the case with no out-of-plane stress, the FE based limit loads for the cases of out-of-plane stress considered generally exceed the corresponding analytical values, with limited non-conservatism (less than 5%) in those cases with close to zero net moment acting on the ligament.

ACKNOWLEDGEMENTS

This paper is published by permission of EDF Energy Nuclear Generation Ltd. The assistance of Peter Budden (EDF Energy) is gratefully acknowledged.

REFERENCES

Abaqus version 6.9 (2009). Dassault Systemes, Providence, RI, USA.

Bass, B. R., Bryson, J. W., Theiss, T. J. and Rao, M. C. (1994). "Biaxial loading and shallow flaw effects on crack tip constraint and fracture toughness". *USNRC report NUREG/CR-6132 (ORNL/TM-12498)*.

Jansson, S. (1986). "Fully plastic plane stress solutions for biaxially loaded center-cracked plates", *Journal of Applied Mechanics*, 53 555-560.

Jones, D. L., Poulose, P. K. and Liebowitz, H. (1986). "The effects of biaxial loading on the fracture characteristics of several engineering materials", *Engineering Fracture Mechanics*, 24 187-205.

Kim, Y.-J., Chung, K.-H., Kim, J.-S. and Kim, Y.-J. (2004). "Effect of biaxial loads on elastic-plastic J and crack tip constraint for cracked plates: finite element study", *International Journal of Fracture*, 130 803-825.

Lee, J. D. and Liebowitz, H. (1977). "The nonlinear and biaxial effects on energy release rate, J-integral and stress intensity factor", *Engineering Fracture Mechanics*, 9 765-779.

Lei, Y. (2014a). "Limit load solutions of plates with surface cracks under combined biaxial forces and cross-thickness bending", EDF Energy Nuclear Generation Ltd. report E/REP/BBGB/0127/GEN/14 Rev 000. (Submitted for publication.)

Lei, Y., Budden, P. and Aird, C. (2014b). "The effect of biaxial loading on the limit load and J estimate for plates with extended surface cracks", *Procedia Materials Science*, 3 667-672.

Lei, Y. and Budden P. J. (2014c). "Limit load solutions of plates with extended surface cracks under combined biaxial forces and cross-thickness bending", *Journal of Strain Analysis for Engineering Design*, 49, 533-54.

Margolin, B. Z. and Kostylev, V. I. (1999). "Analysis of biaxial loading effect on fracture toughness of reactor pressure vessel steels", *International Journal of Pressure Vessels and Piping*, 75 589-601.

Meek, C. and Ainsworth, R. A. (2014a). "Fracture assessment of centre-cracked plates under biaxial loading", *Procedia Materials Science*, 3 1612-1617.

Meek, C. and Ainsworth, R. (2014b). "Ductile fracture assessment of plates under biaxial loading", In *Proceedings of the ASME 2014 Pressure Vessels & Piping Division Conference*, PVP2014-28317, Anaheim, California, USA.

Miura, N. and Takahashi, Y. (2007). "Evaluation of J-integral for surface cracked plates under biaxial loading using extended reference stress method", In *SMiRT 19*, Paper G07/3, Toronto, Canada.

Miura, N. and Takahashi, Y. (2009). "Evaluation of J-integral for surface cracked plates under biaxial tensile/bending loading using extended reference stress method", In *SMiRT 20*, Division II, Paper 1899, Espoo, Finland.

O'Dowd, N. P., Kolednik, O. and Naumenko, V. P. (1999). "Elastic-plastic analysis of biaxially loaded center-cracked plates", *International Journal of Solids and Structures*, 36 5639-5661.

R6 Revision 4 Amendment 11 (2015). "Assessment of the integrity of structures containing defects", EDF Energy Nuclear Generation Ltd., Gloucester, UK.

Wang, X. (2006). "Fully plastic J-integral solutions for surface cracked plates under biaxial loading", *Engineering Fracture Mechanics*, 73 1581-1595.

Wei, L. and Hadley, I. (2012). "The effect of bi-axial stress on limit loads of structures containing surface-breaking flaws and its influence on structural integrity assessments", In *Proceedings of the ASME 2012 Pressure Vessels & Piping Division Conference*, Toronto, Ontario, Canada.

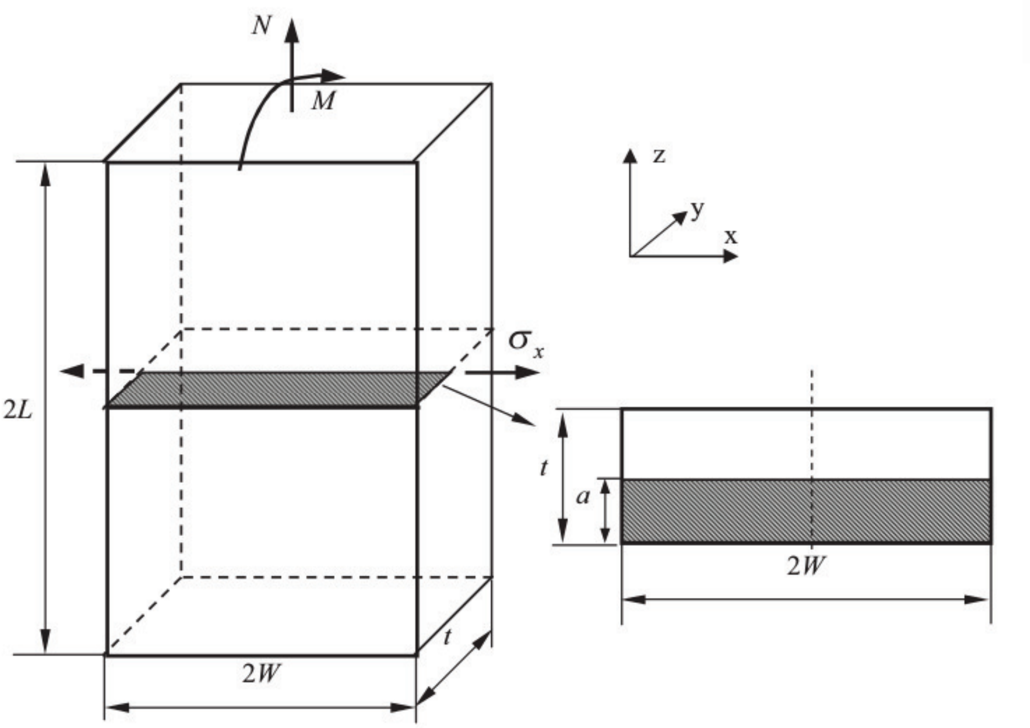

Figure 1. Sketch of cracked plate showing geometry and positive loading directions. The shaded area corresponds to the crack.

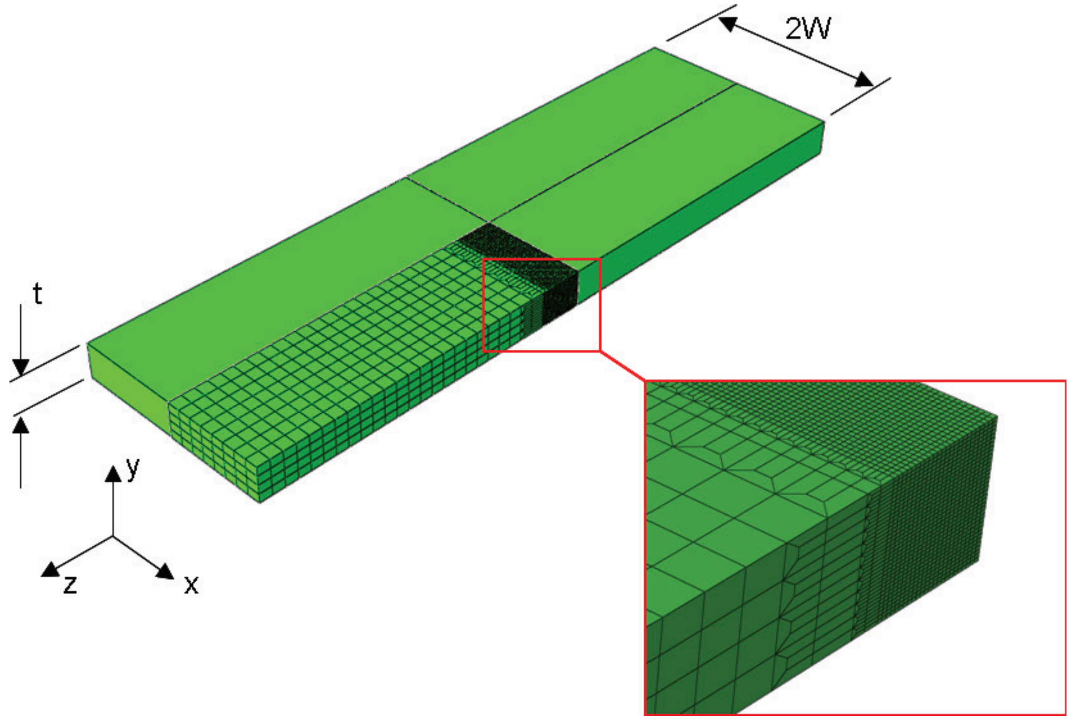

Figure 2. Typical 3D quarter-plate mesh superimposed on the full-sized plate.

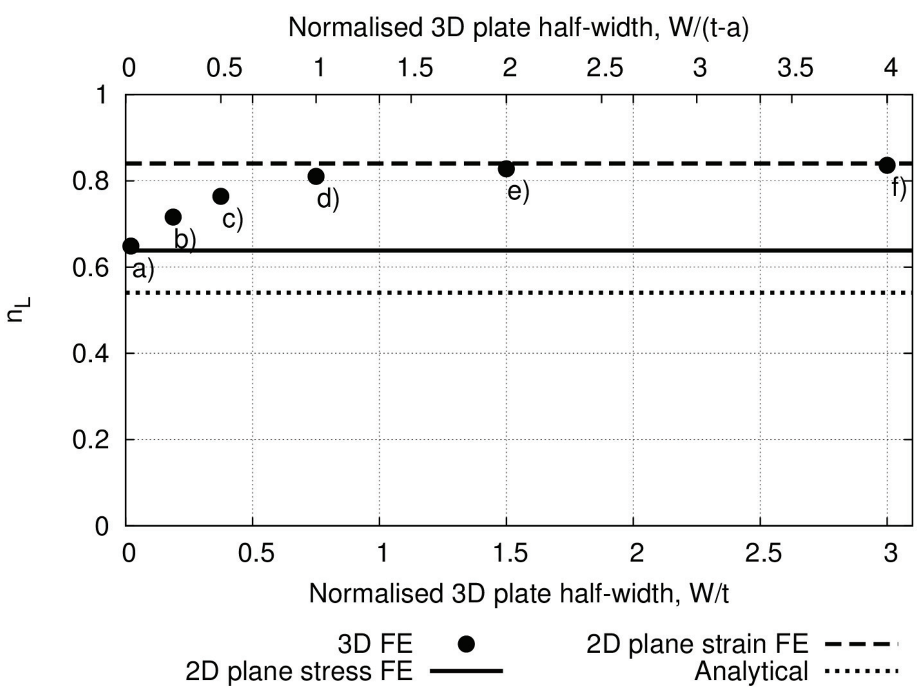

Figure 3. Normalised collapse loads under pure end force predicted by 3D models of varying width –- each with a normalised crack length α of 0.25. Collapse loads predicted using 2D plane stress and 2D plane strain models are shown for comparison along with the analytical collapse load.

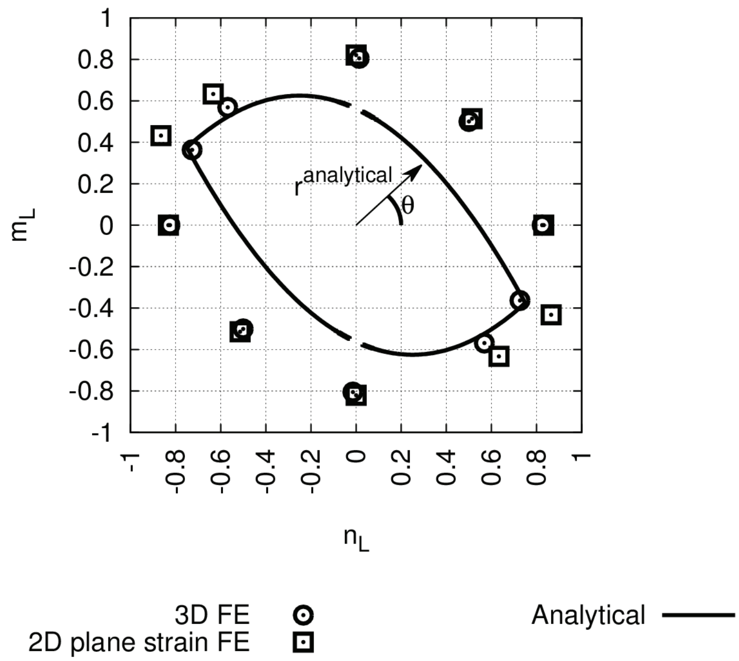

(a) Collapse loci in n_L - m_L space

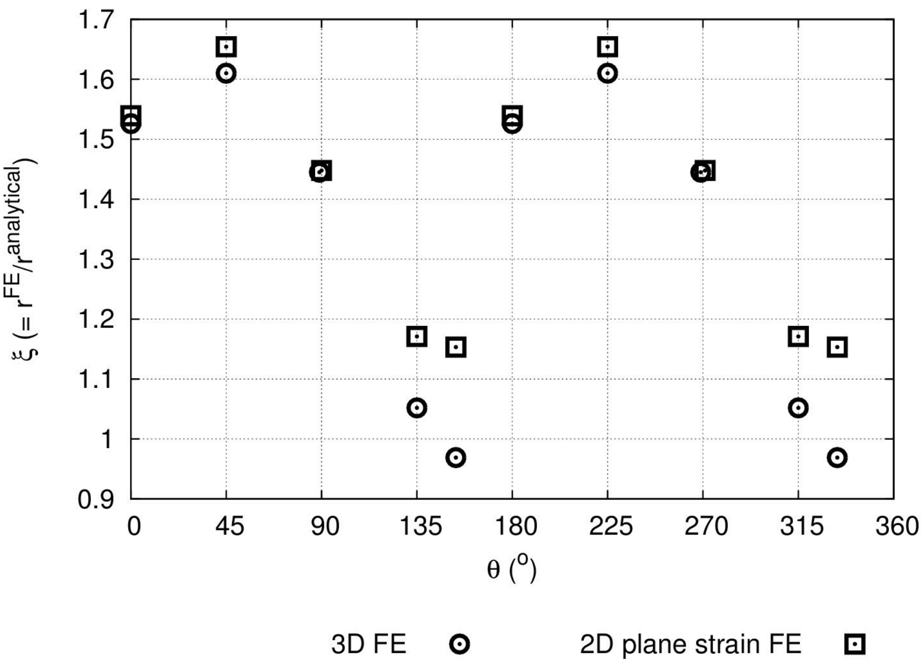

(b) Comparison of FE and analytical collapse loads

Figure 4. 3D model with W/t = 1.5 and α = 0.25 --- comparison of analytical and finite element (wide plate 3D and 2D plane strain) collapse loci with no out-of-plane stress

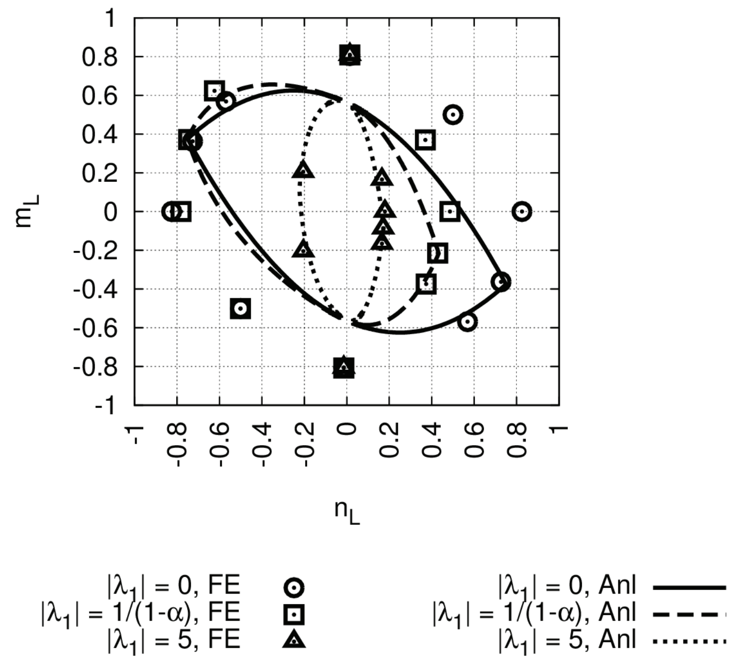

(a) Collapse loci in n_L - m_L space

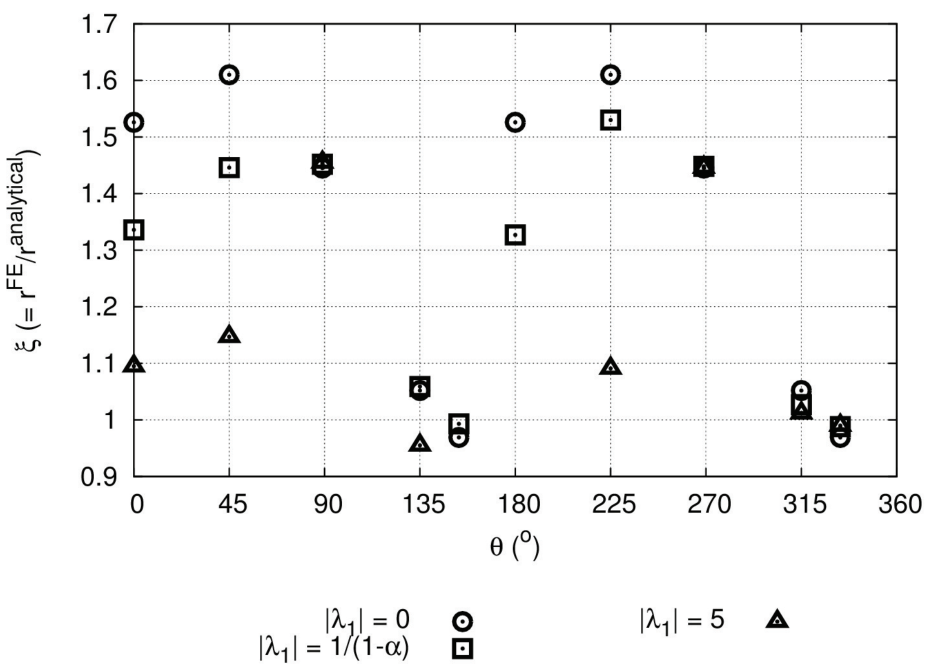

(b) Comparison of FE and analytical collapse loads

Figure 5. 3D model with W/t = 1.5 and α = 0.25 – comparison of analytical and finite element collapse loci with σ_x acting in the negative (compressive) direction in those cases with non-zero λ_1